

Alma Mater Studiorum Università di Bologna
Archivio istituzionale della ricerca

Mass transfer in dilute solid–liquid stirred tanks

This is the final peer-reviewed author's accepted manuscript (postprint) of the following publication:

Published Version:

Carletti, C., Bikic, S., Montante, G., Paglianti, A. (2018). Mass transfer in dilute solid–liquid stirred tanks. *INDUSTRIAL & ENGINEERING CHEMISTRY RESEARCH*, 57(18), 6505-6515 [10.1021/acs.iecr.7b04730].

Availability:

This version is available at: <https://hdl.handle.net/11585/643316> since: 2019-02-22

Published:

DOI: <http://doi.org/10.1021/acs.iecr.7b04730>

Terms of use:

Some rights reserved. The terms and conditions for the reuse of this version of the manuscript are specified in the publishing policy. For all terms of use and more information see the publisher's website.

This item was downloaded from IRIS Università di Bologna (<https://cris.unibo.it/>).
When citing, please refer to the published version.

(Article begins on next page)

This is the final peer-reviewed accepted manuscript of:

Mass Transfer in Dilute Solid–Liquid Stirred Tanks, Claudio Carletti, Siniša Bikić, Giuseppina Montante, and Alessandro Paglianti, *Industrial & Engineering Chemistry Research* 2018 57 (18), 6505-6515

The final published version is available online at:

<https://doi.org/10.1021/acs.iecr.7b04730>

Rights / License:

The terms and conditions for the reuse of this version of the manuscript are specified in the publishing policy. For all terms of use and more information see the publisher's website.

This item was downloaded from IRIS Università di Bologna (<https://cris.unibo.it/>)

When citing, please refer to the published version.

Mass transfer in dilute solid-liquid stirred tanks

Claudio Carletti[†], Siniša Bikić[‡], Giuseppina Montante[†], and Alessandro Paglianti^{§}*

[†]Dipartimento di Chimica Industriale "Toso Montanari", Alma Mater Studiorum – Università di
Bologna, via Terracini 34, 40131 Bologna, Italy

[‡]Faculty of Technical Sciences, University of Novi Sad, Serbia

[§]Dipartimento di Ingegneria Civile, Chimica, Ambientale e dei Materiali, Alma Mater Studiorum
– Università di Bologna, via Terracini 34, 40131 Bologna, Italy

*Corresponding author. Telephone: +390512090403. E-mail alessandro.paglianti@unibo.it

Abstract

This work deals with solid-liquid mass transfer in dilute solids suspension in stirred tanks. The dissolution dynamics of NaCl and CaCl₂ particles in water are determined experimentally in two baffled tanks of similar geometry and different dimensions stirred by standard Rushton turbines, down-pumping Pitched Blade Turbines and Lightnin A310 impellers. The liquid conductivity variation during the salt dissolution is measured locally on four horizontal vessel sections by Electrical Resistance Tomography, thus gaining a detailed picture of the spatial and temporal evolution of the particles dissolution. The analysis of the conductivity time traces leads to calculate the mass transfer coefficient, k_L , as a function of the operating conditions and the stirred tank geometry. Stirring conditions aimed at energy savings are also considered. The

measured k_L ranges from $2.7 \cdot 10^{-5}$ to $1.5 \cdot 10^{-4}$ m/s. Based on the experimental results, a dimensionless correlation for the mass transfer coefficient calculation is proposed and tested for different solids physical properties and agitation conditions under dilute conditions. The correlation matches fairly well the experimental data collected in this work and available in the open literature, being the overall estimated error equal to 19% for tanks stirred by Rushton turbines and its applicability can be easily extended to other impellers.

Introduction

Dissolution of solids in liquids is an important operation in several chemical and pharmaceutical processes. It is often accomplished in stirred tanks of different size and geometry, depending on the specific application. It is well-known that solid liquid mass transfer is dominated by particle size and mixing conditions,¹ but robust mass transfer prediction methods for industrial design and optimization purposes are not available yet. Indeed, several recent works have addressed the importance of a local hydrodynamics characterization of dissolution apparatuses, ranging from mini vessels for dissolution testing systems² to conical stirred tanks for pharmaceutical processes.³ Both experimental techniques (e.g. Particle Image Velocimetry, Laser Doppler Anemometry) and computational methods (mainly Computational Fluid Dynamics) providing local data for a whole field fluid dynamics characterization have started being applied,⁴ while the wider amount of dissolution dynamics data are still mainly based on pointwise experimental methods providing information on single locations. The limitations of single point analysis are well overcome by ERT, which provides information on several locations simultaneously.

Solid-liquid mass transfer has been widely investigated in the past decades. In the 60'-70', the Komogoroff's theory^{5,6} and the slip-velocity theory⁷ have been proposed for modelling mass transfer from particles to agitated liquids. Later, significant efforts have been devoted to verify the validity of the proposed theories for the scale-up of the agitated vessels⁸ and for the identification of tank/impeller configuration effects.⁹ Nienow and Miles (1978)⁹ and Pangarkar et al. (2002)¹⁰ proved that Kolmogoroff's theory leads to a wrong prediction of the effect of the power per unit mass on particle dissolution. According to Nienow and Miles (1978)⁹, the slip

velocity better predicts the experimental results with respect to the Kolmogoroff's theory, while Pangarkar et al. (2002)¹⁰ highlighted that the lack of data on turbulence characteristics especially for large tanks and the difficulty of solving non-linear equations for computing the slip velocity in turbulent flows make the applicability of this approach limited. For the reasons reported above, several authors suggested to determine the mass transfer coefficient by semi-empirical equations or modified Kolmogoroff's theory.¹¹⁻¹⁴ In addition, equations including the dependency from the impeller speed at the just suspended conditions have been proposed.¹⁵

Recently, the importance of a deep analysis of mixing and dissolution in pharmaceutical and chemical processes has been emphasized by many authors.^{4,16-20}

For solid-liquid mass transfer in dilute solids suspension, the just suspended condition might not necessarily be exceeded, since the absence of an unsuspended solid particle layer practically makes almost the whole specific particle surface available for the mass transfer process, even at the beginning of the dissolution. Since the energy requirements strictly depend on the impeller speed, the advantage of working below the just suspended condition might be significant. It is well established that for dilute solid-liquid mixture, the dependency of power consumption from the impeller speed, N , can be assumed proportional to the power of 3. Although a shared theory for mass transfer from solid to liquid in dissolution operations is not achieved yet (the Kolmogoroff's theory, the slip velocity theory or dimensional analysis are alternatively used), the exponent of the impeller speed that most frequently leads to good prediction of mass transfer coefficient data is 0.67.¹⁰ From these experimental evidences, it follows that a moderate decrease of N can lead to significant energy saving with limited impact on mass transfer. For instance, at fixed geometrical characteristics of the tank/impeller, if the impeller speed is reduced of 20% with respect to a reference condition, the power input decreases by about 50% and the

dissolution time increases by 16%, thus leading to a 40% saving of the energy required for the operation. Therefore, in dilute systems, agitation below the so-called just suspended impeller speed, N_{JS} , that is the velocity required for fully suspending the solid particles, might be particularly convenient.²¹ For this reason, in this work the experimental data are collected at N either above and below N_{JS} . Electrical Resistance Tomography (ERT) is adopted, that has the advantage of providing local data on several locations of the vessel without being intrusive. To the best of our knowledge, ERT has never been applied to the investigation of salt dissolution dynamics in agitated liquids so far. The final outcome of the work is the identification of a mass transfer correlation capable of providing reliable results for dissolution in dilute solid-liquid stirred tanks for pharmaceutical and chemical process, covering a wide range of operating conditions, including agitation speeds ensuring energy saving and different vessel dimensions.

Materials and methods

The dissolution of NaCl and CaCl₂ particles in water was carried out in two cylindrical flat-bottomed fully baffled stirred tanks of diameter, T , equal to 0.23 m and 0.48 m, namely T23 and T48 respectively in the following. Both for T23 and T48, agitation was provided by a standard Rushton turbine (RT), a 4-bladed 45° down-pumping Pitched Blade Turbine (PBT) and a Lightnin A310 impeller (A310) placed at a clearance, C , equal to $T/3$ or $T/2$. The main geometrical characteristics of the stirred tanks are summarized in Table 1, where the axial elevations of the four horizontal measurement planes are also provided, together with the size of the electrodes adopted for the ERT measurements.

Table 1. Geometrical details of the stirred tanks and of the electrodes.

	T23	T48
Tank diameter, T [m]	0.23	0.48
Tank Height, H_T	1.2T	3T
Impeller diameter RT, D [m]	0.079	0.151, 0.191
Impeller diameter PBT, D [m]	0.094	0.200
Impeller diameter A310, D [m]	0.096	0.196, 0.252
Impeller clearance, C [m]	0.077, 0.115	0.16, 0.24
Liquid height H_L [m]	0.275	0.569
Baffle width, W	0.023	0.048
Elevation of the measurement planes, z [m]	0.06, 0.11, 0.16, 0.21	0.18, 0.30, 0.42, 0.54
Square electrode side [m]	0.020	0.032
Electrode thickness [m]	0.001	0.002
Number of electrodes per plane	16	16

A schematic illustration of the experimental set-up is depicted in Fig. 1.

Before the salt particles addition, the stirred tanks were filled with slightly salted demineralized water (NaCl concentration equal to 0.086 g/L) up to the height $H_L=1.2T$. With this liquid level, there was not any airspace in the T23 vessel, which was closed with a lid. Instead, a free liquid surface was left in the T48 vessel, which was open on top. The solid phase was added in T23 from the top lid by a hole placed at 11.25° downstream a baffle and midway between the shaft and the vessel wall. Approximately the same location was used in T48.

As the solids, NaCl grains, a single NaCl tablet of cylindrical shape and spherical particles of CaCl_2 were adopted. In all cases, the initial particle volume fraction was well below the value of 10^{-3} , therefore the solid-liquid system is very dilute and the effect of particle-particle interaction can be safely neglected. A narrow size distribution was obtained for the NaCl and CaCl_2 particles

by sieving. The particle mean size adopted in the following, d_p , is the arithmetic mean of the upper and the lower sieve size, as suggested by Nienow (1969)²². In addition, various temperatures and agitation speeds were considered. Details of the salt physical properties and operating parameters are summarized in Table 2.

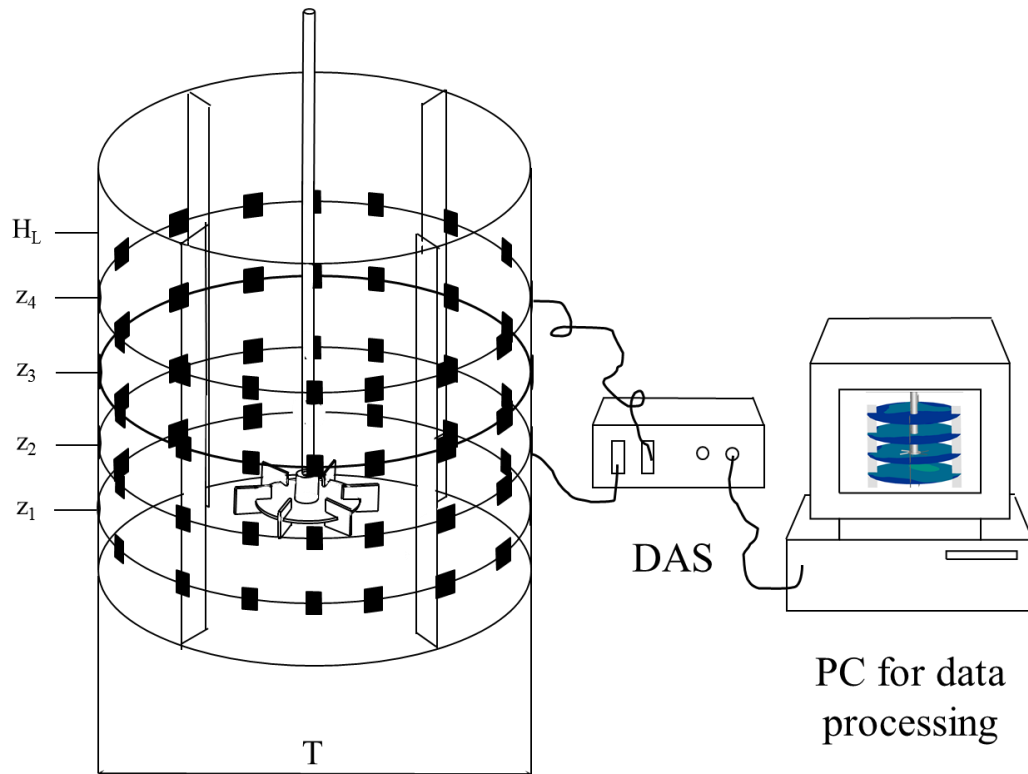


Figure 1 . Sketch of the measurement system.

The salt dissolution dynamics was obtained by the ITS P2000 ERT instrumentation (Industrial Tomography Systems Ltd), by which the distribution of the electrical conductivity in the horizontal sections of the vessel provided with the electrodes was measured as a function of time. The electrodes were arranged at equal intervals around the wall of the vessel, as shown in Figure 1. The measurement is based on the injection of a current between a pair of electrodes and the determination of the resultant voltage difference between the remaining electrodes. Details on

the technique working principles can be found elsewhere.²³ The electrodes were connected to the data acquisition system by co-axial cable for reducing the effect of noise and interference.

The amplitude of 15 mA and the injected current frequency of 9600 Hz were adopted after preliminary calibration tests. The voltage for each recorded frame was determined by the average of 8 instantaneous samples, in order to improve the data accuracy for each frame. The number of recorded frames was varied from 1500 to 3000 depending on the total time required for the complete salt dissolution. In all cases, the acquisition was started 20 seconds before the salt addition. The time resolution of the collected time trace was equal to 0.24 s, resulting from the acquisition of 4.2 frames per second. The local conductivity was obtained from the voltage measurements by adopting the linearized back projection algorithm in real time on a square grid of side equal to 11.5 mm in T23 and to 24 mm in T48. The number of cells per plane was equal to 316 in both cases.

Table 2. Particle properties and relevant investigated conditions.

<i>NaCl particles</i>	<i>T23</i>	<i>T48</i>
Size range, [mm]	0.25-0.6; 1-1.4; 2-4	2-4
Density, [kg/m ³]	2165	2165
Mass, [g]	0.5; 2	4.43; 17.71
Concentration, [g/L]	0.043; 0.172	0.043; 0.172
Impeller speed RT, [rpm]	200, 400, 600, 800	104, 122, 138, 208, 242, 276, 313, 365, 414
Impeller speed PBT, [rpm]	200, 400, 600, 800	100, 150, 200, 250, 300, 350, 400, 450
Impeller speed A310, [rpm]	200, 400, 600, 800	100, 150, 200, 250, 300, 350, 400, 450

Temperature [°C]	12, 20, 30, 45, 60	20
<i>NaCl Tablet</i>	<i>T23</i>	<i>T48</i>
Tablet, height×diameter [mm ²]	8×20	8×20; 5.1×20
Mass, [g]	4.4	4.4; 2.6
Impeller speed RT, [rpm]	400, 600	208, 276, 414
Temperature [°C]	18	18
<i>CaCl₂ particles</i>	<i>T23</i>	<i>T48</i>
Size range, [mm]	4-4.76	4-4.76
Density, [kg/m ³]	1388	1388
Mass, [g]	1	8.86
Concentration, [g/L]	0.086	0.086
Impeller speed RT, [rpm]	200, 400, 600, 800	138, 276
Temperature [°C]	18	18

ERT data treatment for the salt dissolution dynamics determination

The salt dissolution was quantitatively assessed by the analysis of the time trace of the normalized dimensionless conductivity, χ , that on the cell i at the time t is calculated as:

$$\chi_i(t) = \frac{C_i(t) - C_i(0)}{C_i(\infty) - C_i(0)} \quad (1)$$

where the instantaneous dimensionless conductivity on the cell i , $C_i(t)$, is the conductivity at the time t divided by the conductivity of the liquid before the dissolution test, that is adopted as a reference. $t=0$ and $t=\infty$ correspond to the salt addition instant and to the achievement of the complete dissolution, respectively. Since the dimensionless conductivity is affected by temperature variations, the reference conductivity measurement was repeated before each dissolution test, ensuring that the temperature differences with respect to the dissolution conditions were limited to ± 0.2 °C.

In the following, a few examples of the results obtained by different ERT data treatments are provided. The instantaneous normalized conductivity maps shown in Figure 2 for a selected dissolution test allow fully exploiting the local information on each measurement plane, while following the dissolution dynamics. As can be appreciated, after a few seconds from the salt addition ($t=5$ s), χ is higher on the lower plane, on the side corresponding to the position of the partially dissolved salt particles. Afterwards ($t=10$ s), higher values of the mean normalized conductivity are found, the radial gradient are practically negligible except on the higher plane. Later on the dissolution process ($t=40$ s), higher values of χ are measured in all the planes. Finally the normalized conductivity is homogeneous and constant in time across the tank ($t=70$ s), as a result of the complete particle dissolution.

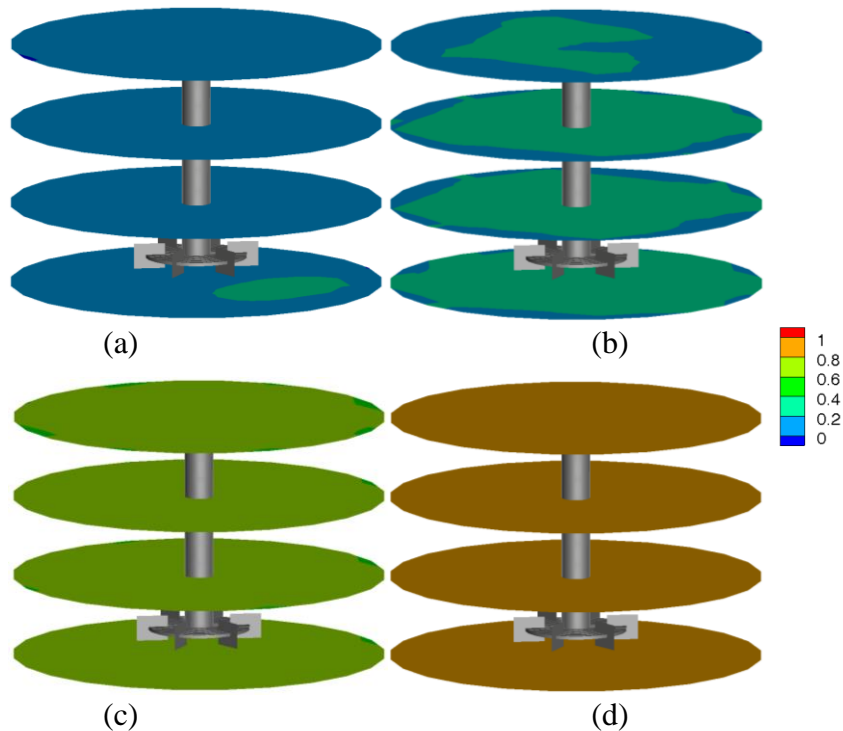


Figure 2. Example of the ERT normalized conductivity maps at selected times during the salt dissolution. T23 RT, $N=400$ rpm, NaCl, $d_p=3$ mm. (a) $t=5$ s; (b) $t=10$ s; (c) $t=40$ s; (d) $t=70$ s.

Generally, in case the local gradients of the dissolved salt concentration are of interest, the post-processing method should be able to maintain the level of detail provided by the technique. To this end, either the visual observation of the 2D conductivity time traces or purposely derived variables can be adopted, as already suggested by Carletti et al. (2016)²⁴ for the analysis of liquid mixing in dense solid-liquid suspensions.

If the effect of different physical or operating variables on the dissolution dynamics is the main investigation target, as is the case of this work, it can be identified from the analysis of the normalized conductivity data averaged on a cross section.

The averaged dimensionless conductivity on each plane was preliminary adopted for assessing the repeatability of the experiments, by comparing the results of triplicate tests in selected conditions both for T23 and T48. As an example, the curves obtained for plane z_1 repeating the dissolution of NaCl under the same conditions are shown in Figure 3. As can be observed, the curves almost overlap thus proving a good repeatability.

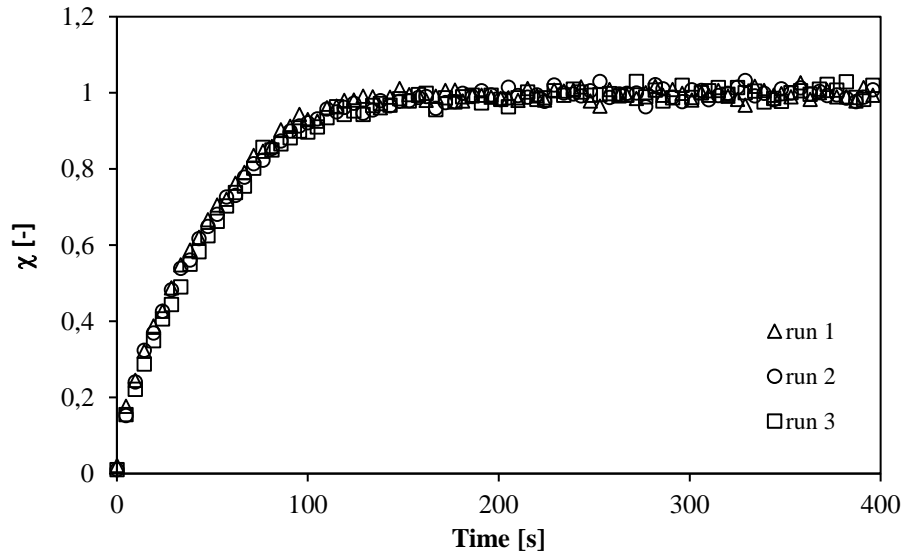


Figure 3 . Averaged dimensionless conductivity on z_1 , $N=138$ rpm, T48 RT, NaCl.

In Figure 4 the average values of χ on the z_3 measurement plane of T23 during the dissolution of NaCl particles of different sizes at the same agitation speed and temperature are shown.

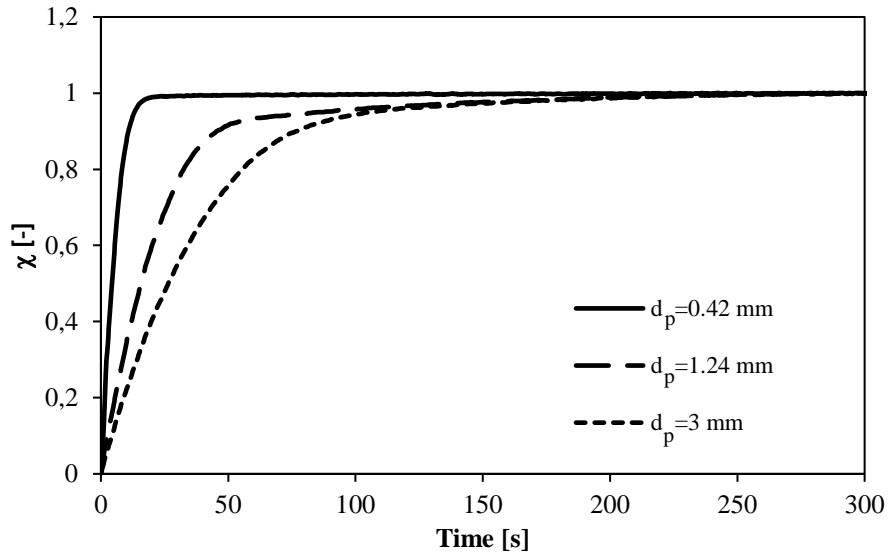


Figure 4 . Time traces of averaged normalized conductivity on z_3 . T23 RT, N=400, NaCl particles.

As can be observed, although the averaged normal conductivity masks the possible local gradients on the plane, it provides a clear indication on the particle diameter effect on the dissolution dynamics and on the overall time required for the process accomplishment. Also, the temperature effect on the dissolution dynamics can be appreciated by a similar data representation, as can be observed from the direct comparison of the dissolution dynamic curves in Figure 5, for three different temperatures. As expected, faster dissolution is obtained increasing the temperature.

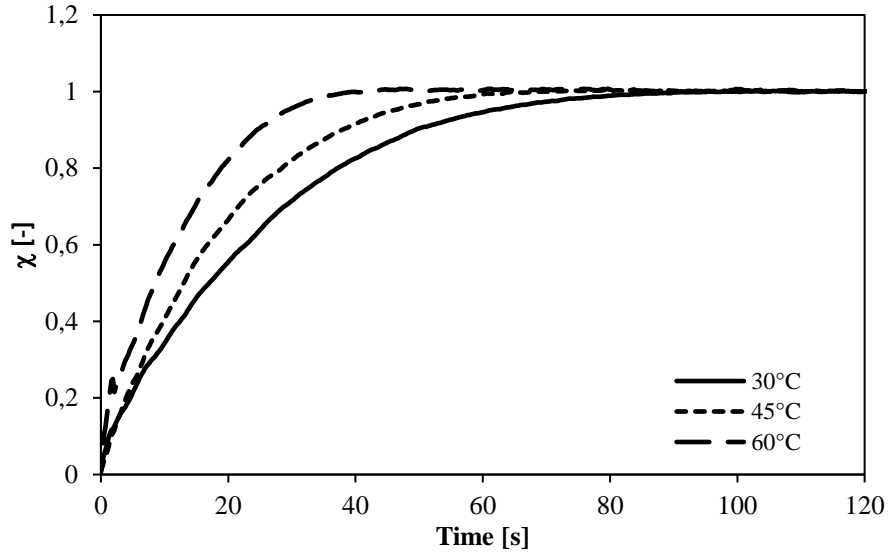


Figure 5. Effect of temperature on the time traces of averaged normalized conductivity on z3. T23 RT, N=200, NaCl particles, $d_p=1-1.4$ mm.

Estimation of the mass transfer coefficient based on the ERT data

The experimental conductivity data are adopted for evaluating the mass transfer coefficient as follows. The volumetric mass flux of a solute from the solid particles to the liquid phase can be described as:

$$\frac{dc_{salt}}{dt} = k_L \cdot a \cdot (c_{salt}^{sat} - c_{salt}) \quad (2)$$

where c_{salt} and c_{salt}^{sat} are the concentration and the solubility of the dissolved salt respectively, k_L is the mass transfer coefficient and a is the particle surface area per unit of volume of solution. The mass transfer coefficient is assumed constant during the dissolution process, because the analyzed particles have diameter greater than $200\mu m^7$, while a is a time dependent variable, that for spherical particles at the generic time t is equal to:

$$a = \frac{6}{d_p} \frac{c_s}{\rho_s} \quad (3)$$

where c_s , d_p and ρ_s are the particles concentration, diameter and density respectively. Under the assumption that the number of particles does not change during the dissolution, the particle diameter d_p can be related to the initial values d_{p0} and c_{s0} as:

$$d_p = d_{p,o} \cdot \sqrt[3]{\frac{c_s}{c_{s,o}}} \quad (4)$$

As a result, equation (3) can be rewritten as:

$$a = \frac{6}{d_{p0}} \frac{c_s}{\rho_s} \sqrt[3]{\frac{c_{s,o}}{c_s}} \quad (5)$$

Finally, after introducing equation (5) into equation (2), the mass flux can be calculated as:

$$\frac{dc_{salt}}{dt} = k_L \cdot \frac{6c_s}{\rho_s d_{p,o}} \cdot \sqrt[3]{\frac{c_{s,o}}{c_s}} \cdot (c_{salt}^{sat} - c_{salt}) \quad (6)$$

The mass transfer coefficient, k_L , is estimated by fitting equation (6) to each of the four experimental curves of the dissolved salt concentration, separately. As a result, four different k_L values are obtained for each experimental condition. The experimental salt concentration curves are obtained from the measured dimensionless conductivity curves, converted with a calibration relationship. A constant value of the mean initial diameter $d_{p,o}$ is adopted due to the narrow size range of the sieved particles. For industrial applications tackling wider size range, this assumption might be not appropriate, as already observed in previous investigations.²⁰

The comparison between the experimental and the calculated time evolution of the salt concentration in the liquid phase on the vessel cross section located at the z_1 is depicted in Figure 6 for the dissolution of NaCl and CaCl₂ in T23. As can be observed, equation (6) closely follows the experimental time traces, both for NaCl and CaCl₂ particles.

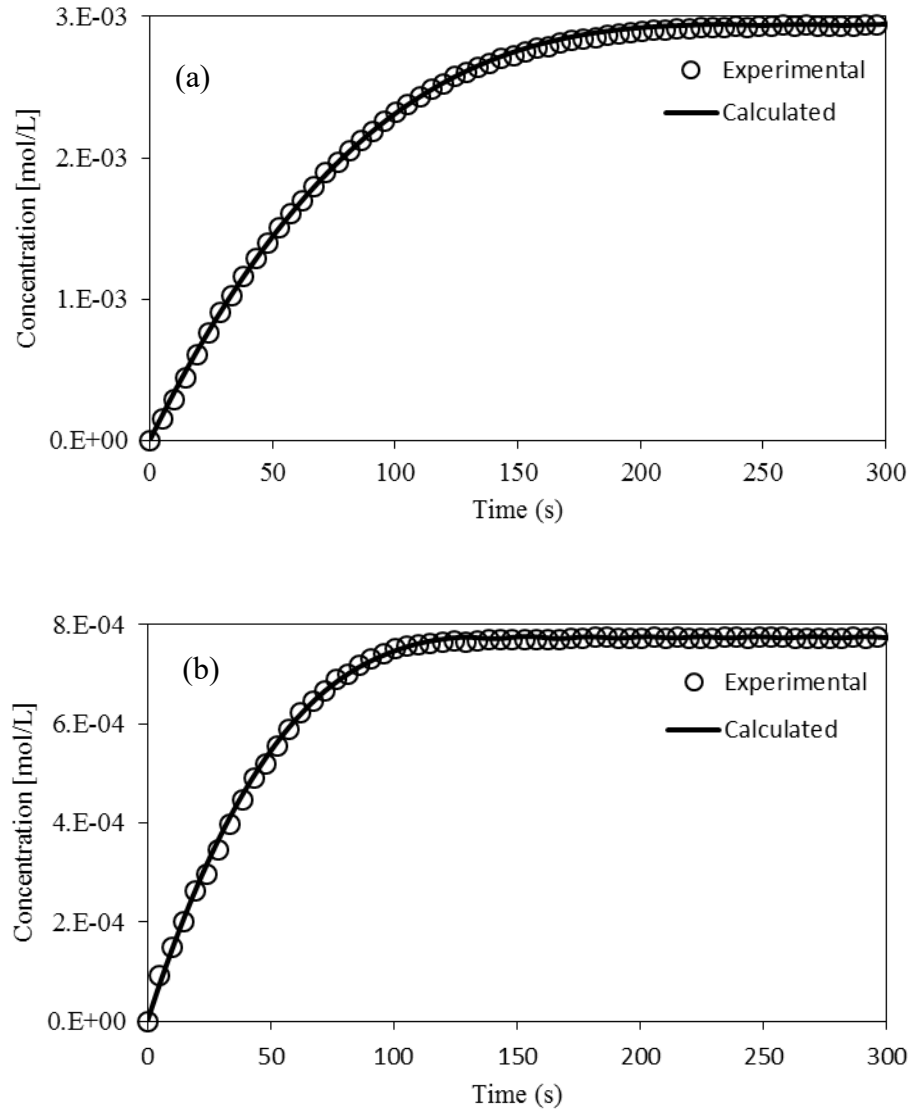


Figure 6 . Measured and calculated salt dissolution dynamics. (a) NaCl, 2 g, $2\text{ mm} < d_p < 4\text{ mm}$, T23, RT, z_1 , $N=200\text{ rpm}$; (b) CaCl₂, 1 g, $4\text{ mm} < d_p < 4.76\text{ mm}$, T23, RT, 200 rpm.

The estimated error on the mass transfer coefficient, based on triplicate measurements, is equal to 3% for the CaCl₂ particles and to 9% and 4% in T23 and in T48, respectively, for the NaCl particles.

Results and discussions

In the following, the results will be presented and discussed with the main aim of identifying a dimensionless equation for the calculation of the mass transfer coefficients in dilute solid-liquid suspensions at impeller speeds either above or below the just suspended conditions of the undissolved particles. In addition to the original data obtained in this work, data collected in previous investigations will be considered for widening the benchmark for the equation.

For covering both complete and incomplete solid suspension conditions, the just suspended impeller speed, N_{js} , was identified approximately by visual observation. Predictive methods, such as the well-known Zwietering correlation, do not hold true for volume fraction below 2 % vol.¹ For the $d_p=3\text{mm}$ NaCl particles, N_{js} was estimated approximately equal to 600 rpm in T23 and to 360 rpm in T48 for agitation by RT of $D=T/3$ located at $C=T/3$. Lower values were observed with the other two impellers.

It is worth observing that if at the beginning of the process N is fixed below N_{js} , the particles shrinkage ensures their suspension, which is lagged with respect to the dissolution onset depending on the initial size and the mass transfer rate. For concentrated solid-liquid systems, the time required for achieving the complete particle dissolution is also a function of the amount of solids sitting on the tank bottom, therefore the conclusions drawn for the dilute conditions could not hold true.

Based on the procedure described in the previous section, four values of the mass transfer coefficient for each investigated condition were obtained, with an average coefficient of variation on each plane of 7%. Due to the limited variations measured in the vessel volume, the following data analysis is based on the mean of the four k_L values. It is worth observing that with the application of ERT, the adoption of a single k_L value is experimentally justified rather than

being just a simplified assumption, as was the case of data collected with simpler pointwise techniques.

The dependency of the mass transfer coefficient on the specific power input and on the impeller tip speed is depicted in Figures 7(a) and 7(b), respectively, considering all the data collected in the two vessels with the three impeller types and the dissolving NaCl particles of mean diameter equal to 3 mm. The classical representation based on the relevant dimensionless numbers is adopted. The k_L data are included in the dimensionless term $(Sh-2) Sc^{-0.33}$, where the Sherwood and the Schmidt numbers are evaluated as $Sh = \frac{k_L d_p}{D_j}$, $Sc = \frac{\mu}{\rho_l D_j}$, respectively. The specific power input, ε , and the impeller tip speed, πND , are included in two different definitions of the Reynolds number, Re_k and Re_p , that are based on the Kolmogoroff theory and on the dimensionless analysis, respectively. As already reported in several previous works, Re_k is defined as $Re_k = \frac{\rho_l d_p^{4/3} \varepsilon^{1/3}}{\mu}$, where overall power input per unit mass, ε , was computed from the impeller power numbers. The Reynolds number definition including the impeller tip speed was firstly introduced by Lal et al.¹² as $Re_p = \frac{\rho_l \pi N D d_p}{\mu}$.

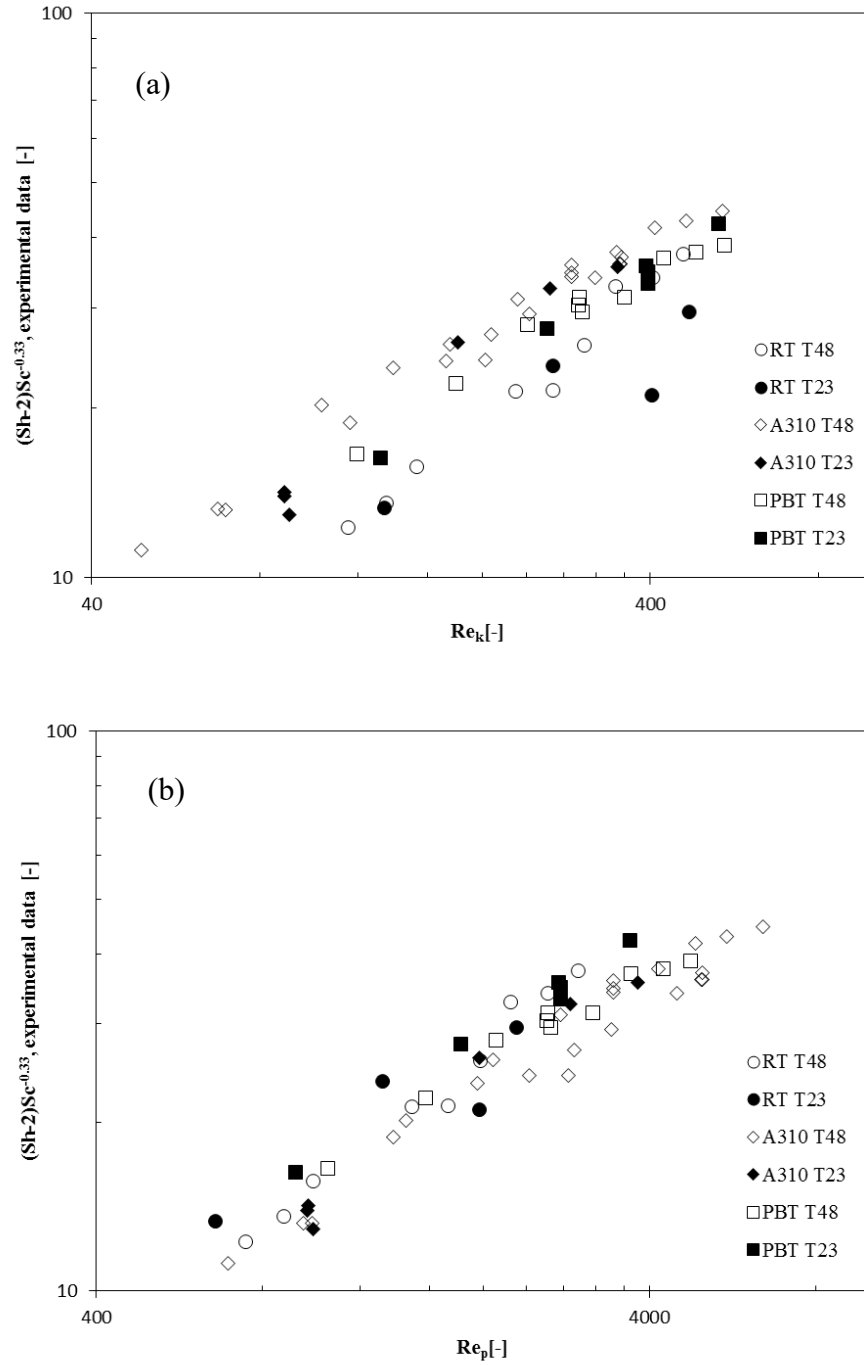


Figure 7. $(Sh-2) Sc^{-0.33}$ as a function of: (a) Re_k , (b) Re_p . NaCl particles in the two investigated vessels. NaCl, 2 g, $2\text{mm} < d_p < 4\text{ mm}$.

As shown in Figure 7(a), at the same power input different Sherwood numbers are measured depending on the impeller type. These results confirm that the Kolmogoroff's theory-based correlations may lead to large errors, at least in the specific range of conditions analyzed in this work, in agreement with the conclusions of Pangarkar et al. (2002)¹⁰. It is worth observing that a proper application of the Kolmogoroff's theory would require a local estimation of the turbulent dissipation rate, that varies dramatically in the vessel volume²⁵, but this is not possible in the realm of global parameter correlations.

The dependency of k_L on Re_p shown in Figure 7(b) highlights that also the terminal velocity theory does not strictly apply to the particle dissolution conditions investigated in this work, because the product $(Sh-2) Sc^{-0.33}$ obtained from the experimental data varies with ND. Instead, if the terminal velocity theory would be accurate, for equal particles $(Sh-2) Sc^{-0.33}$ should be constant with ND.²⁶ In order to widen the applicability of the mass transfer correlation based on the slip velocity theory, the effect of the agitation conditions must be accounted for. As already pointed out by Pangarkar et al. (2002)¹⁰ and confirmed by the present experimental data, the use of the slip velocity theory requires the determination of a characteristic particle-fluid velocity that depends on the turbulent conditions. Instead, we propose to further analyze the relationship between k_L and Re_p , considering the analogy between momentum transfer and mass transfer proposed originally by Friend and Metzner (1962)²⁷ and successively implemented by Hughmark (1974)²⁸, for application to stirred tanks. If the Schmidt number is larger than one, Hughmark²⁸ simplified the equation by Friend and Metzner²⁷ as:

$$\frac{k_L}{V_f} \propto Sc^{-2/3} \sqrt{f/2} \quad (7)$$

where V_f is the characteristic velocity and f is the friction factor.

For N lower than N_{js} , the particles are either still or in slow motion on the vessel bottom, therefore the characteristic velocity, V_f , can be assumed as the liquid velocity on the vessel bottom. This velocity, at fixed geometrical conditions in turbulent regime is proportional to the impeller tip speed. Rearranging Equation (7) to express it as a function of Sh and Re_p numbers, it follows that:

$$Sh \propto Re_p Sc^{1/3} \sqrt{f/2} \quad (8)$$

Where Sh and Sc numbers have the usual meaning and the Reynolds number coincides with the Re_p . In the case of particles suspension, f is the particle drag coefficient. Following Molerous (2000)²⁹, for buoyancy and gravity dominated systems, the drag coefficient can be expressed as function of a ratio between the Archimedes number, $Ar = \frac{g d_p^3 \rho_l (\rho_s - \rho_l)}{\mu^2}$, and the square of the Reynolds number. The Archimedes number was also considered by Brian et al.⁵, who found an overall effect of less of seven percent on the mass and heat transfer coefficients.

Following this simplified approach, Eq. (8) becomes:

$$Sh \propto Re_p^\beta Sc^{1/3} Ar^\alpha \quad (9)$$

To compare the results obtained by Equation (9) with those of previous correlations, the work by Lal et al. (1988)¹² has been used as a reference, since it considered both the Re_k and the Re_p definitions. In particular, the following equations by Lal et al. (1988)¹² are considered:

$$Sh_p = 2 + 0.47 Re_k^{2/3} Sc^{1/3} \quad 1 < Re_k < 800 \quad (10)$$

$$Sh_p = 2 + 0.088 Re_p^{2/3} Sc^{1/3} \quad Re_p < 10^4 \quad (11)$$

which include the range of both Re_k and Re_p investigated in this work. It is worth observing that Lal's et al.¹² adopted the classical definition of Re_k , but the specific energy dissipation rate was explicitly written as a function of the power number N_p . For fixed geometrical characteristics of the stirred tank in turbulent regime, the N_p value is constant, therefore the Re_k can be rewritten:

$$Re_k = \frac{ND^{5/3}d_p^{4/3}\rho_l}{T^{2/3}H_L^{1/3}\mu}. \text{ Equations (10) and (11) have been compared with the final form derived}$$

from Equation (9), as follows:

$$Sh = 2 + \varphi Re_p^{2/3} Sc^{1/3} Ar^\alpha \quad (12)$$

The exponents of Re_p and Sc number have been assumed equal to that defined by Lal et al.¹² Moreover, the constant 2 has been added to account for the mass transfer occurring at very low Reynolds number.

For spherical particles the characteristic size adopted in the dimensionless Archimedes number coincides with the mean particle diameter, as for the Reynolds and the Sherwood numbers. For the cylindrical shape particles, a different definition is required, due to the different physical meaning of the three dimensionless numbers. For Re_p and Sh the diameter of a sphere with the volume to area ratio of the particle is used, while for Ar the hydraulic diameter is considered. In this case, the settling velocity was estimated considering the disk approximation, since for the cylindrical particles used in this work, the ratio between length and diameter is lower than one.³⁰

Finally, the following model constants are obtained by the best fit of the data with the RT at $C/T=0.33$: $\alpha=0.16$ and $\varphi=0.0096$, therefore the final form of Equation (12) is:

$$Sh = 2 + 0.0096 Re_p^{2/3} Sc^{1/3} Ar^{0.16} \quad (13)$$

It is useful to highlight that by this model formulation, the global dependence of Sh from d_p is with an exponent of 1.15, that is consistent with the value suggested by Nienow (1975).²⁶ From the Sh number definition, for the considered working conditions that are relevant to high Re_p values, it follows that k_L is proportional to d_p to the power of 0.15. Therefore, k_L shows a weak dependence from d_p .

The capability of Equation (13) to match the data collected in this work and previous literature data is further investigated by the comparison shown in Figure 8. In particular, the results collected for different particles dissolution in water filled tanks stirred by either standard Rushton Turbines^{9,31,32} or four-bladed Rushton Turbine³³ are considered. In all cases, the impeller diameter and the impeller clearance were equal to $T/3$.

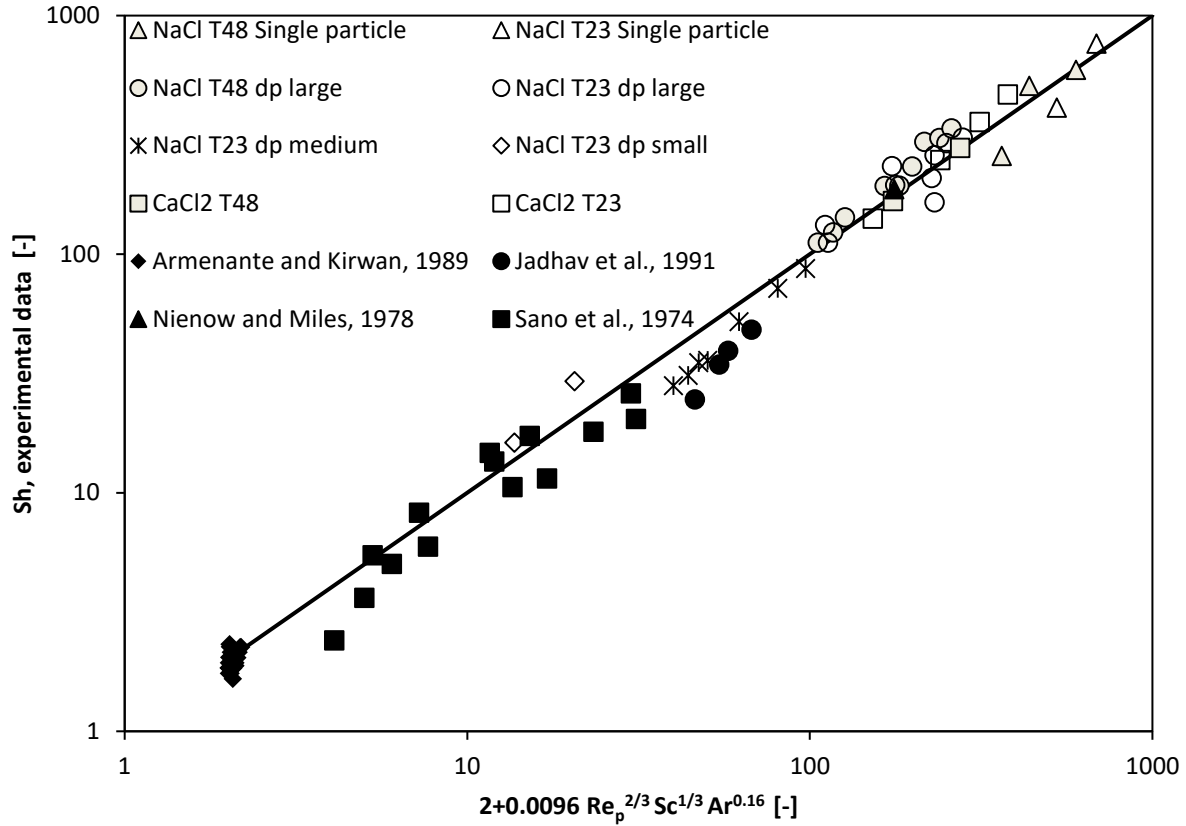


Figure 8. Comparison between equation (13) and the experimental data collected in this and previous works, RT, C/T=1/3, D/T=1/3.

As can be observed, a fair match of the different experimental results is obtained. The mean error for this work and literature data is equal to 17% and 18%, respectively. It is worth observing that different physical properties of the dissolved solids are considered. Indeed, Nienow and Miles (1978)⁹ adopted sodium chloride crystal of 2230 μm mean size stirred at N_{JS} ; Jadhav and Pangarkar (1991)³³ used 655 μm benzoic acid particles stirred at N both above and below N_{JS} ; Sano et al. (1974)³¹ adopted KMnO_4 particles of size in the range of 82-331 μm . As for Armenante and Kirwan (1989),³² the data relevant to microcrystals of AgCl only are included.

In Figure 9, the same experimental data considered in Figure 8 and the results obtained with Equation 10 are compared. A larger scatter of the results with respect to that provided by the correlation suggested in this work is apparent. The estimated mean error for the present and literature data is equal to 28% and 32%, respectively. If the comparison is performed with Equation 11 the mean error obtained for the present and the literature data is equal to 52% and 200%, respectively.

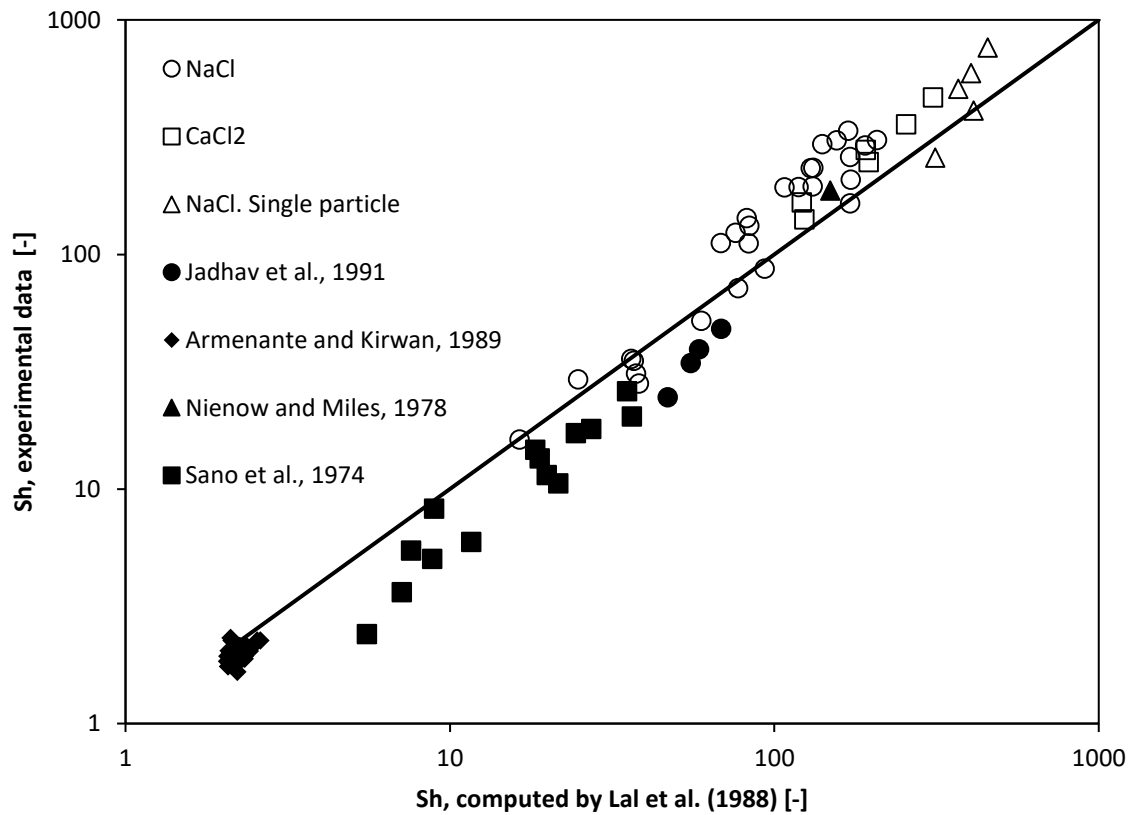


Figure 9. Comparison between the Sh number obtained by experiments and computed by the Equation (10). RT , $C/T=1/3$, $D/T=1/3$.

As a result, Equation (13) is able to match different sets of experimental data collected with different particle sizes and salt physical properties much better than the previous correlations.

Since the characteristic velocity was taken equal to the liquid velocity at the tank bottom, systems with different geometrical characteristics require a different value of the multiplying constant, 0.0096, adopted in Equation (13).

In the following, two different conditions are considered, depending on the impeller type. For axial or mixed flow impellers, the impeller discharge stream impinges the tank bottom directly, therefore it can be considered as a turbulent free jet. When the jet path is lower than 5D, it can be considered in a “region of flow establishment”³⁴ and its velocity is about the same as the initial discharge velocity. Therefore, for axial impeller, Equation 13 can be used without any correction. With radial impellers, the liquid discharge stream reaches the tank bottom after impinging on the later wall. Therefore, for non-standard D/T and C/T values, a correction for V_f is required, due the different decay of the axial velocity components. Following Bittorf and Kresta (2000)³⁵, who demonstrated that the axial velocity components decay linearly with the axial coordinate, the liquid velocity is calculated as follows:

$$V_f \propto \pi N D \left(\frac{D}{C} \right) \quad (14)$$

As a result Equation (13) becomes:

$$Sh = 2 + 0.0096 \left(\frac{D}{C} \right)^{2/3} Re_p^{2/3} Ar^{0.16} Sc^{1/3} \quad (15)$$

The adequacy of Equation (15) for non-standard RT configurations is considered in Figure 10. As can be observed, acceptable results are obtained, being the mean error equal to 20%, for very different systems. In particular, Grisafi et al. (1998)³⁶ adopted potassium sulphate particle of

diameter equal to 1840 μm , Barker and Treybal (1960)³⁷ adopted boric acid particles of size range 0.92-2.88 mm in tanks of diameter ranging from 0.14 to 0.76 m, while Nienow and Miles (1978)⁹ worked with chloride crystals of 2.23 mm in two closed vessels of 0.143 and 0.286 m diameter. It is worth noticing that if the same data are correlated with Eq. 10, based on the Kolmogoroff theory, the mean error is equal to 36%.

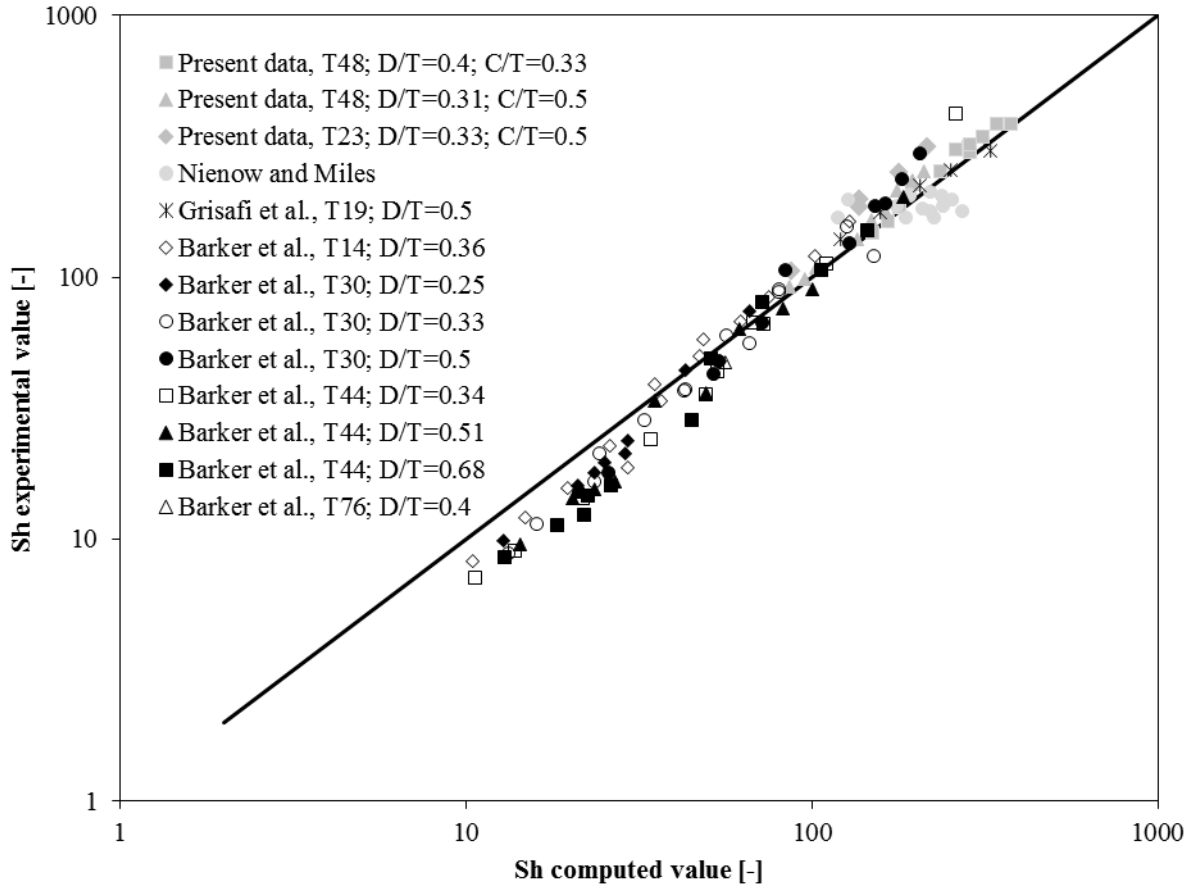


Figure 10. Comparison between Equation (15) and experimental data collected with non-standard RT configurations.

So far the comparison between experimental and computed data has been data limited to tanks stirred by RT. In Figure 11, the evaluation of the applicability of Equation (13) is extended to

different impellers, without any modification of the model constants. In particular, the following experimental data available in the open literature are considered: Nienow and Miles (1978)⁹ data, obtained with down-pumping PBTs, and Jadhav and Pangarkar (1991)³³ data, obtained with up-pumping PBTs.

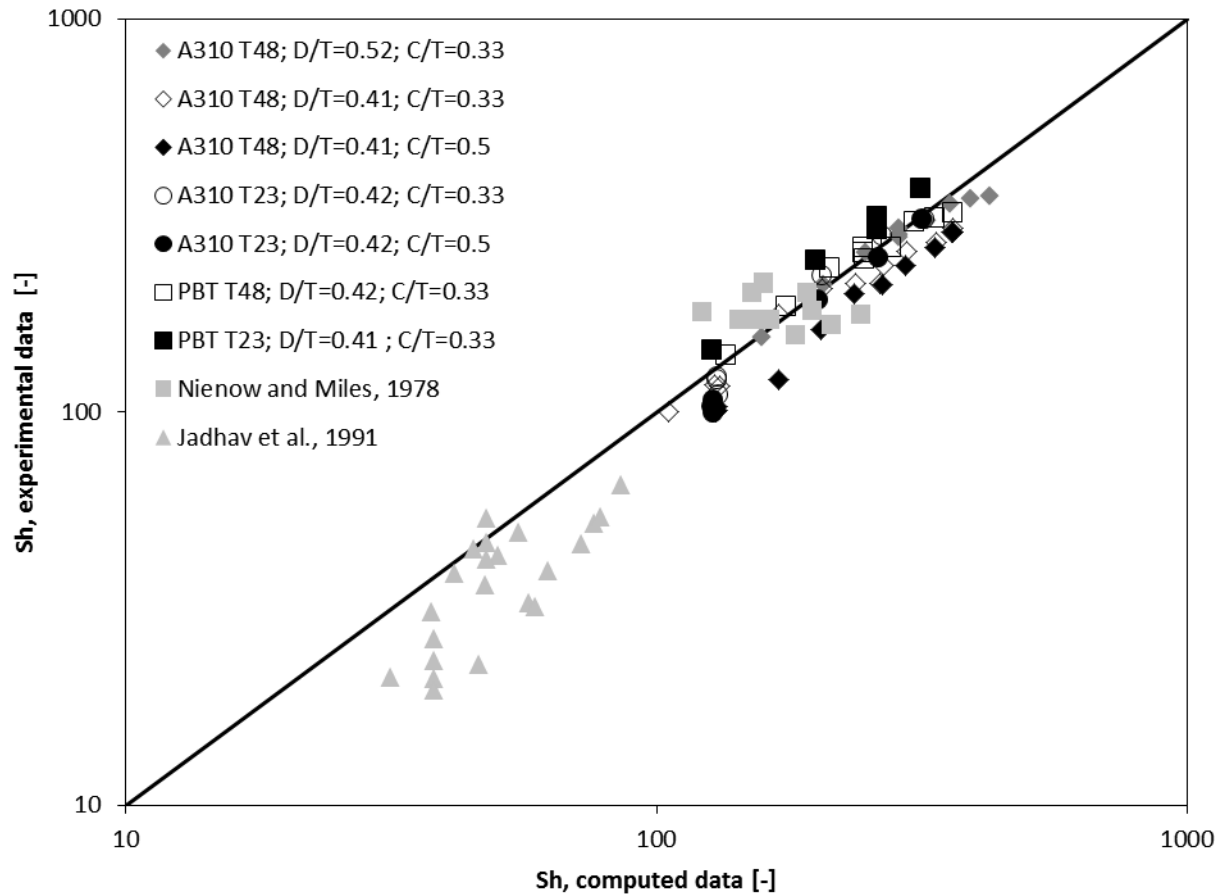


Figure 11. Comparison between Equation (13) and experimental data collected with A310, and PBT.

The comparison shown in Figure 11 highlights that Equation 13 is applicable also for tanks stirred by axial impellers, as the A310 is, or mixed flow impellers, as the PBT. The larger scatter observed for the data due to Jadhav et al.³³ could be due to the up-pumping impeller mode. With reference to the data collected in this work, the mean error for A310 and PBT stirred tanks are equal to 14% and 9%, respectively.

Conclusions

Particles dissolution in stirred tanks for chemical and pharmaceutical operations has been experimentally characterized by ERT, limiting the analysis to the case of dilute solid-liquid systems. For these applications, impeller speeds below N_{JS} might be used because, practically, the whole specific particle surface is available for the mass transfer process, even if the particles are not fully suspended initially. If the stirred tank works at N lower than that required for the initial full suspension of the particles, significant reduction of the energy required for the process can be achieved. The experimental data collected in this work confirm that neither the Kolmogoroff theory or the particle settling velocity theory can be used for the accurate prediction of k_L in equipment of different sizes. Finally, a dimensionless equation based on the analogy between momentum and mass transfer is proposed. The covered dimensionless numbers ranges are: Re_p , $3 \cdot 10^2$ - $4 \cdot 10^4$, Sc , $1.4 \cdot 10^2$ - $1.1 \cdot 10^3$, Ar , $6 \cdot 10^2$ - $6 \cdot 10^5$, Sh , 16 - $1.3 \cdot 10^3$. This equation can be used for the calculation of the mean mass transfer coefficients obtained in tanks of different geometrical characteristics stirred by radial, mixed flow and axial impellers.

Acknowledgements

The stay of S.B. at the University of Bologna was financially supported by the EU, Sunbeam program, in the Erasmus Mundus Action 2 – Strand 1. The contribution of Ms. Francesca Versini in carrying out part of the experimental program is gratefully acknowledged.

Notation

a = particle surface area per unit volume (m^{-1})

Ar = Achimedes number $\frac{g d_p^3 \rho_l (\rho_s - \rho_l)}{\mu^2} (-)$

C = Clearance (m)

c_i = dimensionless conductivity in the cell i (-)

c_s = salt particles concentration (g/L)

c_{salt} = salt concentration in the bulk fluid (g/L)

D = impeller diameter (m)

D_j = diffusion coefficient of species j (m^2/s)

d_p = mean particle diameter (m)

g = gravity acceleration (m/s^2)

H_L = liquid height (m)

k_L = mass transfer coefficient (m/s)

N = impeller speed (1/s)

P = Power consumption (W)

Re_p = particle Reynolds number $\frac{\pi N D d_p \rho_l}{\mu}$ (-)

Re_k = particle Reynolds number based on Kolmogoroff theory $\frac{\rho_l d_p^{4/3} \varepsilon^{1/3}}{\mu}$ (-)

Sc = Schmidt number $\frac{\mu}{\rho_l D_j}$ (-)

Sh = Sherwood number $\frac{k_L d_p}{D_j}$ (-)

t = time (s)

T = tank diameter (m)

V_f = characteristic liquid velocity (m/s)

z_i axial coordinate of the measurement planes (m)

Subscripts and apaxes

o = initial variable, parameter

sat = saturated conditions

∞ = in the bulk fluid.

Greek symbols

ε = power input per unit mass (W/kg)

ρ_l = liquid density (kg/m³)

ρ_s = particle density (kg/m³)

μ = liquid dynamic viscosity (Pa s)

χ = normalized dimensionless conductivity (-)

References

- (1) Paul, E. L.; Atiemo-Obeng, V. A.; Kresta, S. M. *Handbook of Industrial Mixing: Science and Practice*; John Wiley & Sons, 2004.
- (2) Wang, B.; Armenante, P. M. Experimental and Computational Determination of the Hydrodynamics of Mini Vessel Dissolution Testing Systems. *Int. J. Pharm.* **2016**, *510* (1), 336.
- (3) Hörmann, T.; Suzzi, D.; Adam, S.; Khinast, J. G. DOE-Based CFD Optimization of Pharmaceutical Mixing Processes. *J. Pharm. Innov.* **2012**, 1.
- (4) Hörmann, T.; Suzzi, D.; Khinast, J. G. Mixing and Dissolution Processes of Pharmaceutical Bulk Materials in Stirred Tanks: Experimental and Numerical Investigations. *Ind. Eng. Chem. Res.* **2011**, *50* (21), 12011.
- (5) Brian, P. L. T.; Hales, H. B.; Sherwood, T. K. Transport of Heat and Mass between Liquids and Spherical Particles in an Agitated Tank. *AIChE J.* **1969**, *15* (5), 727.
- (6) Levins, D. M.; Glastonbury, J. R. Application of Kolmogoroff's Theory to Particle—liquid Mass Transfer in Agitated Vessels. *Chem. Eng. Sci.* **1972**, *27* (3), 537.
- (7) Harriott, P. Mass Transfer to Particles: Part I. Suspended in Agitated Tanks. *AIChE J.* **1962**, *8* (1), 93.
- (8) Miller, D. N. Scale-Up of Agitated Vessels. Mass Transfer from Suspended Solute Particles. *Ind. Eng. Chem. Process Des. Dev.* **1971**, *10* (3), 365.
- (9) Nienow, A. W.; Miles, D. The Effect of Impeller/tank, Configurations on Fluid-Particle Mass Transfer. *Chem. Eng. J.* **1978**, *15* (1), 13.
- (10) Pangarkar, V. G.; Yawalkar, A. A.; Sharma, M. M.; Beenackers, A. Particle- Liquid Mass Transfer Coefficient in Two-/three-Phase Stirred Tank Reactors. *Ind. Eng. Chem. Res.* **2002**, *41* (17), 4141.
- (11) Boon-Long, S.; Laguerie, C.; Couderc, J. P. Mass Transfer from Suspended Solids to a Liquid in Agitated Vessels. *Chem. Eng. Sci.* **1978**, *33* (7), 813.
- (12) Lal, P.; Kumar, S.; Upadhyay, S. N.; Upadhyay, Y. D. Solid-Liquid Mass Transfer in Agitated Newtonian and Non-Newtonian Fluids. *Ind. Eng. Chem. Res.* **1988**, *27* (7), 1246.
- (13) Dib, A.; Makhloufi, L. Mass Transfer Correlation of Simultaneous Removal by Cementation of Nickel and Cobalt from Sulphate Industrial Solution Containing Copper: Part II: Onto Zinc Powder. *Chem. Eng. J.* **2006**, *123* (1), 53.
- (14) Bong, E. Y.; Eshtiaghi, N.; Wu, J.; Parthasarathy, R. Optimum Solids Concentration for Solids Suspension and Solid–liquid Mass Transfer in Agitated Vessels. *Chem. Eng. Res. Des.* **2015**, *100*, 148.

- (15) Nikhade, B. P.; Pangarkar, V. G. Theorem of Corresponding Hydrodynamic States for Estimation of Transport Properties: Case Study of Mass Transfer Coefficient in Stirred Tank Fitted with Helical Coil. *Ind. Eng. Chem. Res.* **2007**, *46* (10), 3095.
- (16) Winterbottom, M.; Fishwick, R.; Stitt, H. Solid-Liquid Mass Transfer and Hydrodynamics in the Hydrogenation of 4-Nitrobenzoic Acid. *Can. J. Chem. Eng.* **2003**, *81* (3–4), 588.
- (17) Lee, T.; Hou, H. J.; Hsieh, H. Y.; Su, Y. C.; Wang, Y. W.; Hsu, F. B. The Prediction of the Dissolution Rate Constant by Mixing Rules: The Study of Acetaminophen Batches. *Drug Dev. Ind. Pharm.* **2008**, *34* (5), 522.
- (18) Tschentscher, R.; Spijkers, R. J. P.; Nijhuis, T. A.; Van Der Schaaf, J.; Schouten, J. C. Liquid- Solid Mass Transfer in Agitated Slurry Reactors and Rotating Solid Foam Reactors. *Ind. Eng. Chem. Res.* **2010**, *49* (21), 10758.
- (19) El-Naggar, M. A.; Abdel-Aziz, M. H.; Zatout, A. A.; Sedahmed, G. H. Liquid-Solid Mass Transfer Behavior of a Stirred-Tank Reactor with a Fixed Bed at Its Bottom. *Chem. Eng. Technol.* **2014**, *37* (9), 1525.
- (20) Carletti, C.; Blasio, C. D.; Mäkilä, E.; Salonen, J.; Westerlund, T. Optimization of a Wet Flue Gas Desulfurization Scrubber through Mathematical Modeling of Limestone Dissolution Experiments. *Ind. Eng. Chem. Res.* **2015**, *54* (40), 9783.
- (21) Dittl, P.; Rieger, F.; Roušar, I. *The Design of Agitated Dissolution Tanks*. In: King R. (eds) *Fluid Mechanics of Mixing. Fluid Mechanics and Its Applications*, vol 10. Springer, Dordrecht, 1992.
- (22) Nienow, A. W. Dissolution mass transfer in a turbine agitated baffled vessel. *Can. J. Chem. Eng.* **1969**, *47*, 248.
- (23) Dickinson, F.; Wang, M. Electrical resistance tomography for process applications. *Meas. Sci. Technol.*, **1996**, *7*, 247.
- (24) Carletti, C.; Montante, G.; De Blasio, C.; Paglianti, A. Liquid Mixing Dynamics in Slurry Stirred Tanks Based on Electrical Resistance Tomography. *Chem. Eng. Sci.* **2016**, *152*, 478.
- (25) Baldi, S.; Yianneskis, M. On the Direct Measurement of Turbulence Energy Dissipation in Stirred Vessels with PIV (2003) *Ind. Eng. Chem. Res.*, **2003**, *42* (26), 7006.
- (26) Nienow, A. W. Agitated Vessel Particle-Liquid Mass Transfer: A Comparison between Theories and Data. *Chem. Eng. J.* **1975**, *9* (2), 153.
- (27) Friend, W.L.; Metzner, A.B. Turbulent heat transfer inside tubes and the analogy among heat, mass, and momentum transfer *AIChE J.* **1958**, *4*, 393.
- (28) Hughmark, G.A. Hydrodynamics and mass transfer for suspended solid particles in a turbulent liquid. *AIChE J.* **1974**, *20*, 202.
- (29) Molerus, O. Fluid Mechanics in Terms of Eigenparameters: Part II: Exemplary Applications. *Chem. Eng. Sci.* **2000**, *55* (6), 1179.
- (30) Clift, R.; Grace, J. R.; Weber, M. E. *Bubbles, Drops and Particles*; Academic Press: London, 1978.
- (31) Sano, Y.; Yamaguchi, N.; Adachi, T. Mass Transfer Coefficients for Suspended Particles in Agitated Vessels and Bubble Columns. *J. Chem. Eng. Jpn.* **1974**, *7* (4), 255.
- (32) Armenante, P. M.; Kirwan, D. J. Mass Transfer to Microparticles in Agitated Systems. *Chem. Eng. Sci.* **1989**, *44* (12), 2781.
- (33) Jadhav, S. V.; Pangarkar, V. G. Particle-Liquid Mass Transfer in Mechanically Agitated Contactors. *Ind. Eng. Chem. Res.* **1991**, *30* (11), 2496.
- (34) Boucher, D. F., Alves, G. E. Fluid and Particle mechanics. In *Chemical Engineers' Handbook* V edition, Perry, E., Chilton, C.H., Eds.; McGraw-Hill, 1974, pp 5-20.

- (35) Bittorf, K. J.; Kresta, S. M. Active volume of mean circulation for stirred tanks agitated with axial impellers. *Chem. Eng. Sci.* **2000**, 55 (11), 1325.
- (36) Grisafi, F.; Brucato, A.; Rizzuti, L. Solid-Liquid Mass Transfer Coefficients in Gas-Solid-Liquid Agitated Vessels. *Can. J. Chem. Eng.* **1998**, 76 (3), 446.
- (37) Barker, J. J.; Treybal, R. E. Mass Transfer Coefficients for Solids Suspended in Agitated Liquids. *AIChE J.* **1960**, 6 (2), 289.